Inorg. Chem. **2006**, *45*, 9326–9331

Crystal Structure, Judd–Ofelt Analysis, and Spectroscopic Assessment of a $TmAl_3(BO_3)_4$ Crystal as a New Potential Diode-Pumped Laser near 1.9 μm

Guohua Jia,[†] Chaoyang Tu,* Jianfu Li, Zhenyu You, Zhaojie Zhu, and Baichang Wu

Fujian Institute of Research on the Structure of Matter, State Key Laboratory of Structural Chemistry, National Engineering Research Center for Optoelectronic Crystalline Materials, Chinese Academy of Sciences, Fuzhou, Fujian 350002, People's Republic of China

Received June 8, 2006

$TmAl_3(BO_3)_4$ crystallizes in the trigonal system *R*32 (No. 155) with $a = b = 9.2741(13)$ Å, $c = 7.218(3)$ Å, $\alpha = \beta = 90°$, $\gamma = 120°$, $V = 537.7(2)$ Å^3, $D_c = 4.494$ g cm^{-3}, and $Z = 3$. The absorption spectrum of this crystal was recorded at room temperature. The Judd–Ofelt (J–O) theory was applied to the absorption intensities of $TmAl_3(BO_3)_4$ to obtain the three J–O parameters: $\Omega_2 = 2.40 \times 10^{-20}$ cm^2, $\Omega_4 = 0.48 \times 10^{-20}$ cm^2, and $\Omega_6 = 1.09 \times 10^{-20}$ cm^2. The radiative probabilities, radiative lifetimes, and branching ratios of $TmAl_3(BO_3)_4$ were calculated. The absorption and emission cross sections, together with the potential laser gain near 1.9 μm, were investigated. The potential laser gain curves indicate that the tunability range is about 200 nm.

Introduction

The microchip laser technology, the thickness reduction of the laser crystal to the micrometer range, is an alternative to a complicated fabrication process and critical optical alignment.[1] It requires the development and investigation of crystals with a high density of optically active ions, typically in the $(2-5) \times 10^{21}$ cm^{-3}.[2] Hong et al.[3,4] pointed out that rare-earth (RE) stoichiometric laser materials should possess two structural characteristics: first, there is no local inversion symmetry in these crystals so as not to decrease the probability of radiative transition and, second, the RE-O polyhedrons should be isolated among them in order to decrease the quenching fluorescence process of RE ions. The $TmAl_3(BO_3)_4$ crystal possesses a large Tm^{3+} concentration (5.58×10^{21} cm^{-2}) and isolated TmO_6 polyhedrons, and it is comparable with a $NdAl_3(BO_3)_4$[3,4] crystal and satisfies both of these two crystallographic conditions.

Several Nd- and Yb-stoichiometric laser materials such as NdP_5O_{14},[5,6] $LiNd(PO_3)_4$,[7−10] $KNd(PO_3)_4$,[11] $K_5Nd(MoO_4)_4$,[12] $LiYb(MoO_4)_2$,[2] $YbAl_5O_{12}$ (YbAG),[13,14] and $KYb(WO_4)_2$[15] have been reported. Tm-stoichiometric laser material, to our knowledge, has not been in detailed studies yet. The aim of this paper is to investigate the basic structural characteristics of this crystal and evaluate the spectroscopic parameters such as Judd−Ofelt (J−O)[16,17] intensity, radiative lifetime, branching ratios, emission cross section, and potential laser gain

* To whom correspondence should be addressed. E-mail: tcy@ms.fjirsm.ac.cn. Tel.: +86-591-83711368. Fax: +86-591-83711368.

[†] Present address: Department of Biology and Chemistry, City University of Hong Kong.

(1) Zayhowski, J. J.; Mooradian, A. *Opt. Lett.* **1989**, *14*, 24.
(2) Volkov, V.; Cascales, C.; Kling, A.; Zaldo, C. *Chem. Mater.* **2005**, *17*, 291.
(3) Hong, H. Y.-P.; Dwight, K. *Mater. Res. Bull.* **1974**, *9*, 1661
(4) Hong, H. Y.-P. *Mater. Res. Bull.* **1975**, *10*, 1105.
(5) Weber, H. P.; Damen, T. C.; Danielmeyer, H. G.; Tofield, B. C. *Appl. Phys. Lett.* **1973**, *22*, 534.
(6) Danielmeyer, H. G.; Huber, G.; Kruhler, W. W.; Jeser, J. P. *Appl. Phys.* **1975**, *2*, 335.
(7) Otsuka, K.; Yamada, T. *Appl. Phys. Lett.* **1975**, *26*, 311.
(8) Chinn, S. R.; Hong, H. Y.-P. *Appl. Phys. Lett.* **1975**, *26*, 649.
(9) Otsuka, K.; Yamada, T.; Saruwatari, M.; Kimura, T. *IEEE J. Quantum Electron.* **1975**, *11*, 330.
(10) Nakano, J. *J. Appl. Phys.* **1981**, *52*, 1239.
(11) Parreu, I.; Sole, R.; Cavalda, J.; Massons, J.; Diaz, F.; Aguilo, M. *Chem. Mater.* **2003**, *15*, 5059.
(12) Fernandez, J.; Balda, R. *Opt. Lett.* **2003**, *28*, 1341.
(13) Aus der Au, J.; Sphler, G. J.; Sdmeyer, T.; Paschotta, R.; Hvel, R.; Moser, M.; Erhand, S.; Karszewski, M.; Giesen, A.; Keller, U. *Opt. Lett.* **2000**, *25*, 859.
(14) Patel, F. D.; Honea, E. C.; Speth, J.; Payne, S. A.; Hutcheson, R.; Equall, R. *IEEE J. Quantum Electron.* **2001**, *37*, 135.
(15) Pujol, M. C.; Bursukova, M. A.; Guell, F.; Mateos, X.; Sole, R.; Gavalda, J.; Aguilo, M.; Massons, J.; Diaz, F.; Klopp, P.; Griebner, U.; Petrov, V. *Phys. Rev. B* **2002**, *65*, 165121.
(16) Judd, B. R. *Phys. Rev.* **1962**, *127*, 750.
(17) Ofelt, G. S. *J. Chem. Phys.* **1962**, *37*, 511.

10.1021/ic061025n CCC: $33.50
Published on Web 10/13/2006

Table 1. Crystal Data and Structure Refinement of $TmAl_3(BO_3)_4$

empirical formula	$TmAl_3(BO_3)_4$
temperature	293(2) K
wavelength	0.710 73
diffractometer	Rigaku AFC7
θ range for date collection, deg	3.80−39.79
index ranges	$-13 \le h \le 13$, $-13 \le k \le 2$, $-2 \le l \le 10$
cryst syst	trigonal
space group	*R*32 (No. 155)
unit cell dimens	$a = 9.2741(13)$, $\alpha = 90°$; $b = 9.2741(13)$, $\beta = 90°$; $c = 7.218(3)$, $\gamma = 120°$
density (calcd)	4.494 g cm^{-3}
Z	3
abs coeff	12.835
F(000)	672
cryst size	$0.10 \times 0.10 \times 0.10$ mm^3
reflns collcd	721
indep reflns	644
refinement method	full-matrix least squares on F^2
data/restraints/parameters	644/0/35
GOF on F^2	1.084
R indices (all data)	R1 = 0.0153, wR2 = 0.0404
absolute structure param	−0.027(11)
extinction coeff	0.0089(6)
largest diff peak and hole	+1.748 and −2.587 e $Å^{-3}$

coefficients to provide a predictive understanding of the behavior of this material and give insights into the potential laser application around 1.9 μm.

Experimental Section

The $TmAl_3(BO_3)_4$ crystal has been grown successfully from the $K_2Mo_3O_{10}-B_2O_3$ solvent by the top-seeded solution growth slow-cooling method.[18] The crystal structure was investigated by using a Rigaku AFC7 automatic diffractometer equipped with a graphite monochromator with Mo Kα radiation. One crystal with good reflection quality was chosen for data collection. A total of 721 reflections were collected in the hemisphere of the reciprocal lattice of the hexagonal cell, of which 644 were unique with R(int) = 0.0153. An empirical absorption correction using the program *SADABS*[19] was applied to all observed reflections. The experimental parameters for data collection and refinement are given in Table 1. An empirical absorption correction was applied to all observed reflections. The structure was solved with *SHELXS-97*[20] by direct methods and refined with *SHELXL-97*[21] by full-matrix least-squares techniques with anisotropic thermal parameters for all atoms. The refined atomic positions and isotropic thermal parameters are listed in Table 2. Table 3 presents the atomic coordinates and equivalent anisotropic displacement parameters. The main interatomic distances are displayed in Table 4.

Room-temperature absorption spectra were measured in the range from 300 to 2000 nm by using a Perkin-Elmer UV−vis−near-IR spectrometer (Lambda 35).

Results and Discussion

Crystal Structure. In this compound, there are three kinds of coordinations with O: distorted TmO_6 trigonal prisms, AlO_6 octahedra, and two types of triangular BO_3 groups (shown in Figure 1). Among two types of isolated BO_3 groups, one set of B(2) atoms is perpendicular, which are isosceles triangles with their double-fold rotation axis parallel to the *ab* crystal plane, and the other set of B(1) is nearly so, to the *c* axis. The Al^{3+} and Tm^{3+} ions occupy O octahedral and trigonal prisms, respectively. Edge-shared Al^{3+} octahedra form helices along the *c* axis, with the average distance of Al−O ranging from 1.860(2) to 1.928(2) Å. The Tm^{3+} cations, which are located between adjacent layers of anions, are coordinated to six O(3) atoms; three of them are common to the B(2) borate anions of the layer above and the other three anions with the B(2) borates of the layer below. The Tm−O bands are equally 2.305(2) Å.

Table 2. Final Refined Atomic Position and U_{eq} of $TmAl_3(BO_3)_4$[a]

atom	position	*x*	*y*	*z*	U_{eq} (Å)
Tm(1)	3*a*	1.00000	1.00000	1.00000	0.0063(1)
Al(1)	9*d*	0.8886(2)	1.2219(1)	2/3	0.0037(2)
O(1)	9*e*	1.00000	1.1490(3)	1/2	0.0054(4)
O(2)	9*e*	1.00000	1.4083(4)	1/2	0.0071(5)
O(3)	18*f*	0.8171(3)	1.0334(2)	0.8134(3)	0.0061(3)
B(1)	3*b*	1.00000	1.00000	1/2	0.0049(7)
B(2)	9*e*	1.00000	1.5560(5)	1/2	0.0055(5)

[a] U_{eq} is defined as one-third of the trace of the orthogonalized U_{ij} tensor.

The huntite structure of $TmAl_3(BO_3)_4$ can be viewed as formed by layers normal to the *c* axis (shown in Figure 2), in which there are TmO_6 prisms and smaller AlO_6 octahedra. The three AlO_6 octahedra repeat edge-sharing forms of the infinite helicoidal chains along the *c* axis (shown in Figure 2). TmO_6 polyhedra are interconnected within the layers by corner sharing with two types of BO_3 trigonal groups and AlO_6 octahedra, and the nearest distance between Tm^{3+} ions is as far as 5.870 Å. This unique structure of isolated Tm trigonal prisms will result in a weak interaction and a lower fluorescence concentration quenching effect.[3,4]

Optical Spectroscopy. Because the Tm^{3+}-stoichiometric crystal possesses a high concentration, up to 5.58×10^{21} cm^{-3}, the sample used for absorption measurement must be thin enough (in this case, the thickness of the sample is 0.46 mm) to avoid intense or absolute (100%) absorbance. Figure 3 presents a room-temperature absorption spectrum of the $TmAl_3(BO_3)_4$ crystal. It consists of five groups of bands associated with the transitions from the $^3H_6$ ground state to the $^3F_4$, $^3H_5$, $^3H_4$,$^3F_3$ + $^3F_2$, and $^1G_4$ excited states. The absorption cross section was calculated from the absorption coefficient $\alpha(\lambda)$ using

$$\sigma_a(\lambda) = \alpha(\lambda)/N_o \quad (1)$$

where $\alpha(\lambda) = A(\lambda)/(L \log e)$, $A(\lambda)$ is the absorbance, L is the thickness of the polished sample, and N_o is the Tm^{3+} concentration in ions per cubic centimeters. The absorption band around 800 nm corresponding to the $^3H_6 \rightarrow {}^3H_4$ transition was used to determine the cross section versus wavelength of the pumping (see Figure 3 inset). The peak absorption cross section occurs at 807 nm with a 8-nm full

(18) Jia, G. H.; Tu, C. Y.; Li, J. F.; Zhu, Z. J.; You, Z. Y.; Wang, Y.; Wu, B. C. *Cryst. Growth Des.* **2005**, *5*, 949.
(19) Sheldrick, G. M. *SHELXTL*, version 5; Siemens Analytical Instruments Inc.: Madison, WI, 1994.
(20) Sheldrick, G. M. *SHELXL-97: Program for the solution of Crystal Structure*; University of Gottingen: Gottingen, Germany, 1997.
(21) Sheldrick, G. M. *SHELXL-97: Program for the solution of crystal structures refinement*; University of Gottingen: Gottingen, Germany, 1997.

Table 3. Anisotropic Displacement Parameters (Å^2) of $TmAl_3(BO_3)_4$

atom	U_{11}	U_{22}	U_{33}	U_{12}	U_{13}	U_{23}
Tm(1)	0.00642(8)	0.00642(8)	0.00599(10)	0.00321(4)	0.00000	0.00000
Al(1)	0.0041(3)	0.0041(3)	0.0036(5)	0.0026(3)	0.00023(13)	−0.00023(13)
O(1)	0.0074(9)	0.0050(7)	0.0048(9)	0.0037(5)	0.0011(7)	0.0005(3)
O(2)	0.0087(11)	0.0056(8)	0.0079(12)	0.0044(5)	0.0030(8)	0.0015(4)
O(3)	0.0055(6)	0.0046(6)	0.0065(7)	0.0012(5)	−0.0007(5)	0.0007(5)
B(1)	0.0057(11)	0.0057(11)	0.0034(17)	0.0029(5)	0.00000	0.00000

Table 4. Select Bond Lengths (Å) of $TmAl_3(BO_3)_4$[a]

atom	distance	atom	distance
Trigonal Prisms of TmO_6			
Tm(1)−O(3)#1	2.305(2)	Tm(1)−O(3)#3	2.305(2)
Tm(1)−O(3)#2	2.305(2)	Tm(1)−O(3)#4	2.305(2)
Tm(1)−O3	2.305(3)	Tm(1)−O(3)#5	2.305(3)
Octahedra of AlO_6			
Al(1)−O(3)	1.860(2)	Al(1)−O(1)#9	1.916(2)
Al(1)−O(3)#12	1.860(2)	Al(1)−O(2)#9	1.928(2)
Al(1)−O(1)	1.916(2)	Al(1)−O(2)	1.928(2)
Planar Triangles of BO_3			
B(1)−O(1)#3	1.382(3)	B(2)−O(3)#14	1.374(3)
B(1)−O(1)#2	1.382(2)	B(2)−O(3)	1.374(4)
O(1)−B(1)	1.382(3)	O(2)−B(2)	1.370(6)

[a] Symmetry transformations used to generate equivalent atoms: (#1) x, y, z; (#2) $-y, x-y, z$; (#3) $-x+y, -x, z$; (#4) $y, x, -z$; (#5) $x-y, -y, -z$; (#6) $-x, -x+y, -z$; (#7) $x+{}^2/_3, y+{}^1/_3, z+{}^1/_3$; (#8) $-y+{}^2/_3, x-y+{}^1/_3, z+{}^1/_3$; (#9) $-x+y+{}^2/_3, -x+{}^1/_3, z+{}^1/_3$; (#10) $y+{}^2/_3, x+{}^1/_3, -z+{}^1/_3$; (#11) $x-y+{}^2/_3, -y+{}^1/_3, -z+{}^1/_3$; (#12) $-x+{}^2/_3, -x+y+{}^1/_3, -z+{}^1/_3$; (#13) $x+{}^1/_3, y+{}^2/_3, z+{}^2/_3$; (#14) $-y+{}^1/_3, x-y+{}^2/_3, z+{}^2/_3$; (#15) $-x+y+{}^1/_3, -x+{}^2/_3, z+{}^2/_3$; (#16) $y+{}^1/_3, x+{}^2/_3, -z+{}^2/_3$; (#17) $x-y+{}^1/_3, -y+{}^2/_3, -z+{}^2/_3$; (#18) $-x+{}^1/_3, -x+y+{}^2/_3, -z+{}^2/_3$.

width at half-maximum , and the corresponding absorption cross section is 0.48×10^{-20} cm^2. This moderate absorption cross section is ideal as a microchip laser material because the value is comparable with that of Tm^{3+}:YAG: 0.75×10^{-20} cm^2.[22] A relatively broad absorption band and a high cross section are very promising features for the efficient optical pumping of this system with laser diodes.

The measured absorption line strength S_{exp} for transitions from the ground state to the excited J' level can be obtained from the room-temperature absorption spectrum using the following expression:[23,24]

$$\Gamma = N_J \frac{8\pi^3 e^2 \bar{\lambda}}{3hc} \frac{(n^2+2)^2}{9n} \frac{1}{2J+1} S_{exp} \qquad (2)$$

where N_J is the Tm^{3+} concentration, h is Planck's constant, e is the electron charge, $\bar{\lambda}$ is the mean wavelength of the absorption band, c is the vacuum speed of light, n is the refractive index of this crystal, which is estimated to be 1.75, J is the total angular momentum of the ground state ($J = 6$ in Tm^{3+}), and Γ is the integrated absorbance for each absorption band, which can be defined as

$$\Gamma = \frac{2.303 \int D(\lambda)\, d\lambda}{L} \qquad (3)$$

where L is the crystal thickness and $D(\lambda)\, d\lambda$ is the measured optical density as a function of the wavelength.

On the basis of the J−O theory, the measured line strengths were then used to obtain the J−O intensity parameters Ω_2, Ω_4, and Ω_6 by fitting the set of equations from the corresponding transitions between J and J' manifolds in the following equation:

$$S_{calc}(J \rightarrow J') = \sum_{t=2,4,6} \Omega_t |\langle (S,L)J || U^{(t)\prime} || (S',L')J' \rangle|^2 \qquad (4)$$

where $U^{(t)}$ ($t = 2$, 4, and 6) are the matrix elements of the unit tensor calculated by Carnall et al.[25] Table 5 presents the integrated absorbance and the experimental and calculated line and oscillator strengths. To justify our fitting quality, the root-mean-square (rms) deviation between the experimental and calculated strengths was determined by

$$\text{rms } \Delta S = \sqrt{\sum_{i=1}^{N} (S_{exp} - S_{calc})^2/(N-3)} \qquad (5)$$

The rms error is 0.207×10^{-20} cm^2. A lower rms deviation between the experimental and calculated line strengths confirms a better consistency of our fitting.

After a least-squares fitting of S_{meas} to S_{calc}, the three J−O intensity parameters $\Omega_2 = 2.40 \times 10^{-20}$ cm^2, $\Omega_4 = 0.48 \times 10^{-20}$ cm^2, and $\Omega_6 = 1.09 \times 10^{-20}$cm^2 were obtained, in accordance with those of other existing laser-active media, which are shown in Table 6. As is pointed out,[35] the parameter of Ω_2 is closely related to the covalence and structure changes of the crystal; the higher the value, the stronger the covalence characteristics of the crystal and vice versa. The relatively large value of Ω_2 suggests the weaker ionic characteristics of this crystal.

(22) Fan, T. Y.; Huber, G.; Byer, R. L.; Mitzscherlich, P. *IEEE J. Quantum Electron.* **1988**, *24*, 924.
(23) Krupke, W. F. *Phys. Rev.* **1966**, *174*, 429.
(24) Krupke, W. F. *IEEE J. Quantum Electron.* **1971**, *7*, 153
(25) Carnall, W. T.; Fielsd, P. R.; Wybourne, B. G. *J. Chem. Phys.* **1965**, *42*, 3797.
(26) Tu, C. Y.; Li, J. F.; Zhu, Z. J.; Chen, Z. Q.; Wang, Y.; Wu, B. C. *Opt. Mater.* **2003**, *227*, 383.
(27) Guell, F.; Gavalda, J.; Sole, R.; Aguilo, M.; Diaz, F.; Galan, M.; Masons, J. *J. Appl. Phys.* **2004**, *95*, 919.
(28) Ermeneux, F. S.; Goutaudier, C.; Moncorge, R.; Cohen-Adad, M. T.; Bettinelli, M.; Cavalli, E. *Opt. Mater.* **1997**, *8*, 83.
(29) Ohta, K.; Saito, H.; Obara, M. *J. Appl. Phys.* **1993**, *73*, 3149.
(30) Weber, M. J.; Varitimos, T. E.; Matsinger, B. *Phys. Rev. B* **1973**, *8*, 47.
(31) Payne, S. A.; Chase, L. L.; Smith, L. K.; Kway, W. L.; Krupke, W. F. *IEEE J. Quantum Electron.* **1992**, *28*, 2619.
(32) Krupke, W. F. *Phys. Rev.* **1966**, *145*, 325.
(33) Gruber, J. B.; Krupke, W. F.; Poindexter, J. M. *J. Chem. Phys.* **1964**, *41*, 3363.
(34) Wyba-Romanowski, W.; Golab, S.; Sokolska, I.; Dominiak-Dzik, G.; Zawadzka, J.; Berkowski, M.; Fink-Finowichi, J.; Baba, M. *Appl. Phys. B: Lasers Opt.* **1999**, *68*, 199.
(35) Song, F.; Guo, H. C.; Zhang, W. L.; Shang, M. R.; Shang, G. Y. *Spectrosc. Spectral Anal.* **2000**, *22*, 1 (in Chinese).

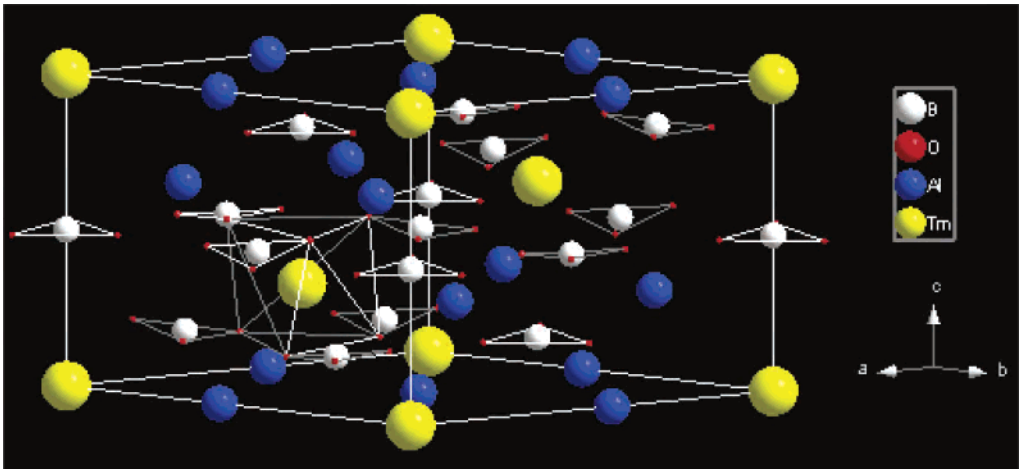

Figure 1. View of the TmO_6 trigonal prism, AlO_6 octahedra, and BO_3 triangle in the structure of $TmAl_3(BO_3)_4$.

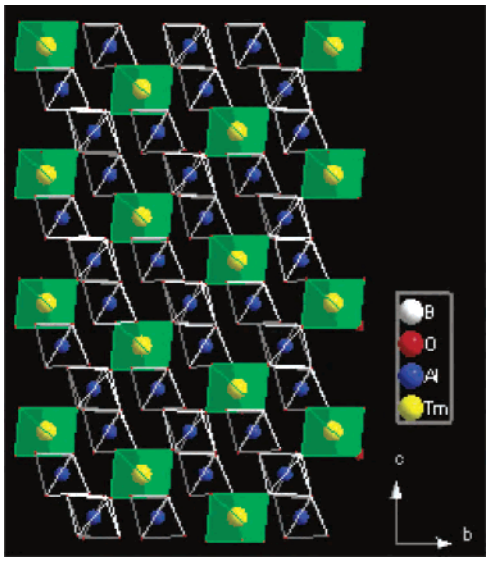

Figure 2. View of the helicoidal chains of the TmO_6 trigonal prism and AlO_6 octahedra parallel to the *c* axis in $TmAl_3(BO_3)_4$.

The J−O intensity parameters were applied to eq 4 to calculate the line strengths. Using the obtained emission line strengths, the radiative decay rates $A(J\rightarrow J')$ can be determined by the following expression:

$$A(J\rightarrow J') = \frac{64\pi^4 e^2}{3h(2J+1)\bar{\lambda}^3}\frac{n(n^2+2)^2}{9} \times \sum_{t=2,4,6} \Omega_t |\langle (S,L)J||U^{(t)}||(S',L')J'\rangle|^2 \quad (6)$$

Then the radiative lifetimes $\tau_r = 1/A_T(J)$; the mathematical formulas for the fluorescent branching ratio were found by

$$A_T(J) = \sum_{J'} A(J\rightarrow J') \quad (7)$$

$$\beta(J') = A(J\rightarrow J')/A_T(J) \quad (8)$$

Table 7 presents the calculated radiative transition rates, the branching ratios, and the radiative lifetimes for different transition levels, which were estimated using parameters and the reduced matrix elements published in ref 36. The lifetime of the $^3F_4$ level is much longer than that of the others, implying that a favorable population inversion can be easily

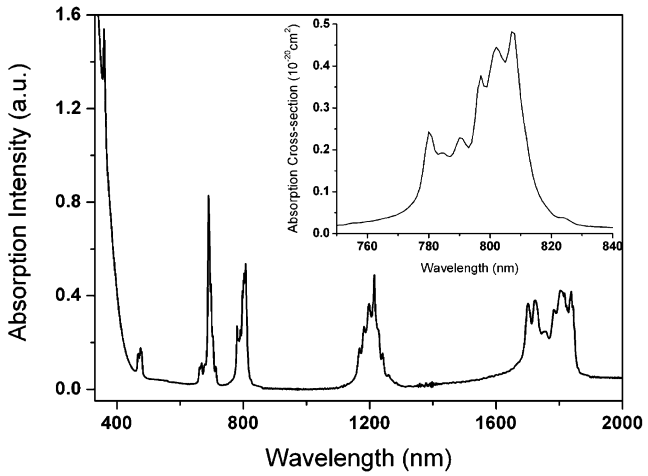

Figure 3. Absorption spectra of the $TmAl_3(BO_3)_4$ crystal recorded at room temperature.

Table 5. Integrated Absorbance and the Experimental and Calculated Line and Oscillator Strengths

excited state	λ (nm)	Γ (nm cm^{-1})	line strength (10^{-20} cm^2)		oscillator strength (10^{-6})	
			S_{exp}	S_{calc}	f_{exp}	f_{calc}
$^3F_4$	1803	2268.71	1.88	1.89	1.41	1.43
$^3H_5$	1215	1113.41	1.37	1.06	1.53	1.18
$^3H_4$	807	620.33	1.15	1.26	1.93	2.12
$^3F_3 + {}^3F_2$	690	567.57	1.23	1.34	2.41	2.63
$^1G_4$	475	73.19	0.23	0.17	0.66	0.47
$^1D_2$	359	47.12	0.20	0.25	0.74	0.95

Table 6. Comparison of the $^3F_4 \rightarrow {}^3H_6$ Emission Cross Section and Radiative Lifetime of the $^3F_4$ State in Different Hosts

crystal	Ω_2	Ω_4	Ω_6	σ_{em} ($\times 10^{-20}$ cm^2)	$\tau[^3F_4]$ (μs)	ref
$KGd(WO_4)_2$	2.64	5.84	14	1.90	1760	26, 27
YVO_4	9	1.05	2.27	1.60	800	28, 29
$Y_3Al_5O_{12}$	0.7	1.2	0.5	0.22	8500	30, 31
Y_2O_3	4.07	1.46	0.61		1318	32, 33
$SrGdGa_3O_7$	1.29	1.08	0.47	0.39	4700	34
$TmAl_3(BO_3)_4$	2.40	0.48	1.09	0.83	7042	this work

Table 7. Stimulated Emission Sections, Calculated Radiative Transition Rates, Branching Ratios, and the Radiative Lifetimes for Different Transition Levels

start level	terminal level	wavelength (nm)	A (s^{-1})	β	τ (μs)
$^1D_2$	$^3H_6$	359	3876	0.230	59
	$^3F_4$	450	11530	0.683	
	$^3H_5$	508	101	0.006	
	$^3H_4$	652	1380	0.082	
	$^3F_3 + {}^3F_2$	758	1205	0.071	
	$^1G_4$	1491	118	0.007	
$^1G_4$	$^3H_6$	473	589	0.366	621
	$^3F_4$	644	132	0.082	
	$^3H_5$	770	640	0.398	
	$^3H_4$	1158	198	0.123	
	$^3F_3 + {}^3F_2$	1543	50	0.031	
$^3F_2$	$^3H_6$	670	69	0.091	1309
	$^3F_4$	1069	486	0.637	
	$^3H_5$	1431	198	0.259	
	$^3H_4$	4215	10	0.013	
	$^3F_3$	17513	0	0.000	
$^3F_3$	$^3H_6$	686	1770	0.855	483
	$^3F_4$	1138	68	0.033	
	$^3H_5$	1558	232	0.112	
	$^3H_4$	5552	1	0.000	
$^3H_4$	$^3H_6$	798	939	0.927	987
	$^3F_4$	1452	65	0.065	
	$^3H_5$	2300	9	0.009	
$^3H_5$	$^3H_6$	1225	195	0.972	4963
	$^3F_4$	4226	5	0.028	
$^3F_4$	$^3H_6$	1771	142	1	7042

achieved. Also, the transition $^3H_4 \rightarrow {}^3H_6$ may accomplish good laser output.

To qualify the 1.9-μm emissions, the reciprocity method (RM)[31,37] was used to determine the emission cross section of the $^3F_4 \rightarrow {}^3H_6$ transition. The RM allows us to determine the emission cross section as a function of the wavelength $\sigma_{em}(\lambda)$ from the known ground-state absorption cross section $\sigma_{abs}(\lambda)$, assuming that Stark level positions of both multiplets are known:[30]

$$\sigma_{em}(\lambda) = \sigma_{abs}(\lambda)\frac{Z_l}{Z_u}\exp\left(\frac{E_{ZL} - hc/\lambda}{k_B T}\right) \quad (9)$$

where $\sigma_{abs} = \alpha/N_o$ is the absorption cross section, N_o is the dopant concentration, Z_l and Z_u are partition functions of the lower and upper levels, respectively, E_{ZL} is the energy between the lowest Stark levels of the multiplets involved, k_B is Boltzmann's constant, and T is the temperature. Here we replace the unknown energies of the crystal-field levels by the energy difference of each part of the spectrum from E_{ZL}. The value of E_{ZL} can be easily determined from the position of the highest absorption peak of Tm^{3+}. However, because of the lack of a low-temperature spectrum, the precise energy scheme of $TmAl_3(BO_3)_4$ cannot be obtained at present. The values of Z_l/Z_u and E_{ZL} were estimated to be 1.39 and 5612 cm^{-1}, respectively, which is on the order of those of Tm^{3+}:$KGd(WO_4)_2$,[27] Tm^{3+}:$La_2Be_2O_5$,[31] Tm^{3+}:BaY_2F_8,[31] Tm^{3+}:$LiYF_4$,[38] Tm^{3+}:$Y_3Al_5O_{12}$,[39,40] Tm^{3+}:LaF_3,[41,42] Tm^{3+}:$KCaF_3$,[43] Tm^{3+}:$YAlO_3$,[44,45] and Tm^{3+}:$KYb(WO_4)_2$ crystals.[46]

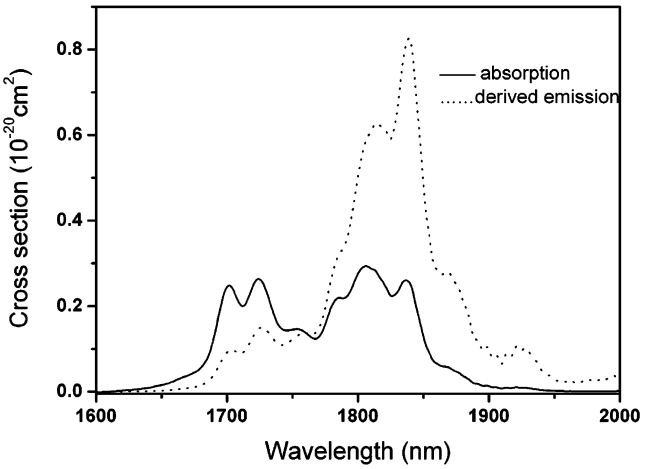

Figure 4. Absorption cross section due to the $^3H_6 \rightarrow {}^3F_4$ transition (solid lines) and the derived emission cross-sectional curves (dotted lines) for the $^3F_4 \rightarrow {}^3H_6$ transition.

The emission cross sections calculated by the RM, together with the absorption cross sections (solid line), are shown in Figure 4. The maximum emission cross section centered at 1.85 μm is 0.83 $\times$ 10^{-20} cm^2. The values of the emission cross section and the radiative lifetime for the $^3F_4$ state are on the order of those reported for other Tm^{3+}-based laser crystals, as shown in Table 6.

The transition of $^3F_4 \rightarrow {}^3H_6$ is a quasi-three-level laser scheme in which the lower level is thermally populated at room temperature. The reabsorption and increase of the threshold may arise during the laser operation. It is of critical important to reduce the reabsorption and maintain the efficient absorption of the pump light in the design of the Tm-doped laser systems on the $^3F_4 \rightarrow {}^3H_6$ transition. [27] From the estimated absorption and emission cross sections of Tm^{3+} in the range of 1.6−2.0 μm, we calculated the gain cross section from the following equation:

$$\sigma_{gain} = P\sigma_{em}(\lambda) - (1 - P)\sigma_{abs}(\lambda) \quad (10)$$

where P is the population inversion rate and σ_{em} and σ_{abs} are the emission and absorption cross sections derived from the RM, respectively. The wavelength dependences of the gain cross section for both π and σ polarizations were calculated in terms of population inversion P (P = 0, 0.1,

(36) Carnall, W. T.; Fields, P. R.; Rajnak, K. *J. Chem. Phys.* **1968**, *49*, 4424.
(37) McCumber, D. E. *Phys. Rev. A* **1964**, *134*, 299.
(38) Jenssen, H. P.; Linz, A.; Leavitt, P. R.; Morrison, C. A.; Wortman, D. E. *Phys. Rev. B* **1975**, *11*, 92.
(39) Gruber, J. B.; Hills, M. E.; Macfarlane, R. J.; Morrison, C. A.; Turner, G. A.; Quarles, G. J.; Kintz, G. J.; Esterowitz, L. *Phys. Rev. B* **1989**, *40*, 9464.
(40) Armagan, G.; DiBartolo, B.; Buoncristiani, A. M. *J. Lumin.* **1989**, *44*, 129.
(41) Huang, S.; Lai, S. T.; Lou, L.; Jia, W.; Yen, W. M. *Phys. Rev. B* **1981**, *24*, 59.
(42) Carnall, W. T.; Fields, P. R.; Morrison, J.; Sarup, R. J. *Chem. Phys.* **1970**, *52*, 4054.
(43) Chen, C. Y.; Sibley, W. A.; Yeh, D. C.; Hunt, C. A. *J. Lumin.* **1989**, *43*, 47.
(44) Weber, M. J.; Varitimos, T. E.; Matsinger, B. H. *Phys. Rev. B* **1973**, *8*, 47.
(45) Antonov, V. A.; Arsenev, P. A.; Beinert, K. E.; Potemkin, A. V. *Phys. Status Solidi A* **1973**, *19*, 289.
(46) Bagaev, S. N.; Vatnik, S. M.; Maiorov, A. P.; Pavlyuk, A. A.; Plakushchev, D. V. *Quantum Electron.* **2004**, *30*, 310.

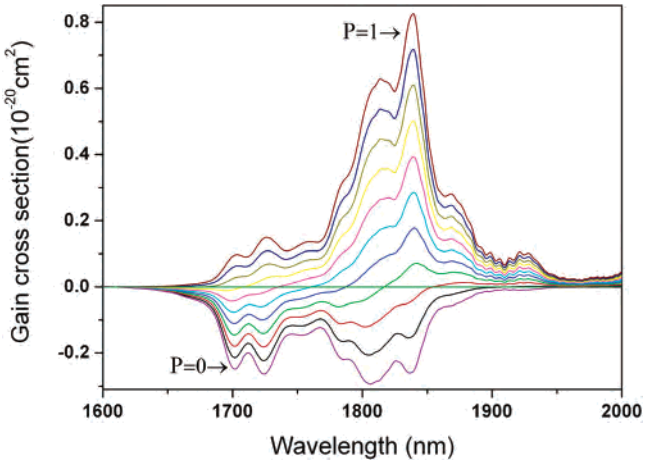

Figure 5. Gain cross section calculated for different values of P for the $^3F_4 \rightarrow {}^3H_6$ transition.

0.2, ..., 1) and are shown in Figure 5. The population inversion rate needed to achieve application is expected to be higher than 0.1. For a population inversion level of 0.3, the gain is produced in the 1.82−2.0-μm spectral region. This wavelength range corresponds to the absorption bands of liquid water and water vapor.[47] High P can be achieved by high-power pulse pumping with the ground-state-depleted operation.[48] The higher energy limit of this interval increased when the population inversion level was increased, reaching up to 1.76 μm for a population inversion level of 0.5. For this level, the maximum gain cross-sectional value centered at 1.84 μm is 2.85×10^{-21} cm^2. Laser experiments for this emission are expected to find light amplification in the future at this point.

On the basis of the spectra of the absorption and emission cross sections (derived by the RM) between the ground state and the lowest excited state displayed in Figure 4, the extracted efficiency for laser application, which is strongly dependent on the operating wavelength, can be determined:[31,48]

$$f_{\max}(\lambda) = \frac{\sigma_{em}(\lambda)}{\sigma_{em}(\lambda) + \sigma_{abs}(\lambda)} = \frac{1}{1 + \frac{Z_u}{Z_l}\exp\left(\frac{\frac{hc}{\lambda} - E_{ZL}}{kT}\right)} \quad (11)$$

The energy difference between the photon energy and the zero line, $hc/\lambda - E_{ZL}$ is, in part, related to the energy of the terminal laser level above the ground state. From this simple exercise, we obtain $f_{\max} = 0.42$, 0.54, 0.66, 0.76, 0.84, and 0.90, for $E_{ZL} - hc/\lambda = 0$, 103, 206, 309, 412, and 515 cm^{-1} ($kT = 206$ cm^{-1}), respectively. To ensure a reasonable efficiency for extraction, the energy difference between the photon energy and the zero line, $\Delta E = E_{ZL} - hc/\lambda$, must be greater than 300 cm^{-1}.

Conclusion

The crystal structure of $TmAl_3(BO_3)_4$ has been refined and analyzed. The intensity parameters, oscillator intensities, radiative transition probabilities, and radiative lifetimes, together with the branching ratios, were calculated according to the J−O theory. The stimulated emission cross sections calculated by the RM were compared with those of other Tm^{3+}-doped materials and discussed. The optical gain versus wavelength for several populations in conversion rates was estimated, and the analysis of the gain coefficient implies the possible laser tunability in the range from 1.82 to 2.0 μm for the $^3F_4 \rightarrow {}^3H_6$ transition. Large emission cross sections and broad possible laser oscillation (nearly 200 nm) suggest that the $TmAl_3(BO_3)_4$ crystal may be regarded as a potential diode-pumped solid-state 1.9-μm laser medium.

The Tm^{3+} concentration in this crystal is estimated to be up to 5.58×10^{21} cm^{-3}. At such high ion concentrations, energy-transfer processes will most probably play a significant role in the population mechanisms of the Tm^{3+} ions. There is possibly a considerable difference between the calculated potential laser gain and the experimental one. Future studies should employ time-resolved techniques to investigate energy-transfer processes and explain it based on the resonant interaction theory.[49]

Acknowledgment. This work was supported by Innovative Project of CAS (Project KJCX2-SW-h05), NSF of Fujian Province of China (Grant E0410028), and Frontier & Interdisciplinary project of Fujian Institute of Research on the Structure of Matter, CAS. We thank Dr. Jian Zhang, Xinyi Cao, and Jianrong Li at the Fujian Institute of Research on the Structure of Matter, Chinese Academy of Sciences, for refining the CIF file.

Supporting Information Available: X-ray crystallographic files (CIF format). This material is available free of charge via the Internet at http://pubs.acs.org.

IC061025N

(47) Yamanouchi, T.; Tanaka, M. *J. Quant. Spectrosc. Radiat. Transfer* **1985**, *34*, 463.
(48) Krupke, W. F.; Chase, L. L. *Opt. Quantum Electron.* **1990**, *22*, S1.
(49) Kellendonk, F.; Blasse, G. *J. Chem. Phys.* **1981**, *75*, 561.